Model-scale PIV measurements of the far-wake of a frigate

Miloš Birvalski[1*], Rink Hallmann[2], Johan Bosschers[2]

1: Performance at Sea dept., MARIN, The Netherlands
2: Defence dept., MARIN, The Netherlands
* Correspondent author: m.birvalski@marin.nl

Keywords: model-scale measurements, stereo-PIV, wake hydrodynamics, frigate, wakefield

ABSTRACT

This study presents model-scale stereo Particle Image Velocimetry (PIV) measurements of the wake evolution behind a twin-screw frigate hull, with particular emphasis on the far-wake region. While previous studies have predominantly focused on near-wake flow structures, far-wake measurements remain scarce despite their importance for understanding wake persistence, signature characteristics, and propulsor–wake interaction. To address this gap, a basin-fixed stereo-PIV system was deployed in MARIN's deepwater towing tank to acquire velocity fields up to 12 ship lengths downstream of the model. A generic frigate model was tested under four configurations. The PIV system measured three velocity components in a large transverse plane, enabling detailed characterization of the flow. Measurements were performed at a towing speed of 1.9 m/s, with multiple runs and varying PIV inter-frame times to resolve both high-velocity gradients near the propellers as well as lower velocities in the far wake. The results demonstrate a clear evolution of the wake structure from a highly organized propeller-dominated flow near the stern to a more diffuse and dissipated flow in the far wake. Powered cases exhibit strong recirculating and rotational features that decay with distance, while the unpowered configuration shows a symmetric, forward-directed flow without pronounced vortex structures. Differences between configurations highlight the influence of propeller loading and rudder presence on wake topology and turbulence levels. Although measurement uncertainties are influenced by calibration limitations, seeding quality, and a finite number of runs, the mean velocity fields are considered sufficiently reliable for comparison with CFD. The dataset provides valuable insight into the far-wake behavior of naval vessels and serves as a benchmark for future validation studies and hydrodynamic design optimization.

1. Introduction

Since the early demonstrations of PIV in a towing tank, numerous studies have successfully applied 2D and 3D PIV to ship hydrodynamics looking at boundary layers, nominal wakes, propeller–hull interactions, etc. Pioneering work established the feasibility of wake measurements using PIV in a towing tank ([1], [2]), while subsequent studies expanded the technique to more

complex flow configurations (e.g. [3], [4], [5], [6], [7]). These investigations confirmed that PIV is a reliable tool for wake measurements in controlled basin environments.

Most existing PIV wake studies have focused on commercial ship hull forms, such as container vessels, tankers, and bulk carriers. In contrast, PIV measurements of wakes behind surface combatant hulls (such as frigates) remain relatively limited. Surface combatants differ from merchant vessels in terms of hull slenderness, stern geometry, appendage arrangement and operating speed, all of which strongly influence wake structure. For these vessels, specific interest is placed on overall signature, so quantifying wake characteristics is of great importance. While some PIV studies have addressed nominal wakes of generic surface ships [1], [8], most measurements are concentrated in the near-wake region close to the stern. These are typically done using carriage-fixed PIV systems. Measuring in the far-wake which extends multiple hull lengths (L_{pp}) downstream, however, is of interest for surface combatants because the relevant phenomena (e.g. wake recovery, propulsor–wake interaction, signature persistence) are visible only in the far-wake. Basin-fixed PIV systems offer a practical approach for such measurements, allowing repeatable acquisition of wake planes at different downstream locations relative to the ship.

The present study employs a basin-fixed stereo-PIV system to measure the wake of a model-scale frigate hull, with emphasis on the evolution of the wake into the far-wake region. The resulting velocity fields provide insight into wake development behind surface combatants and constitute a valuable reference for numerical model validation and future naval hydrodynamic design studies.

2. Measurement setup

Ship model

The 'Generic frigate' model of MARIN is sufficiently representative of the hull shape of vessels in the existing naval fleet that the insights obtained from measurements are relevant. The model is fitted with five-bladed propellers and double rudders, as well as bilge keels and a trim control device (Figure 1). The model tests were conducted in the Deepwater Towing tank (DT), which measures 250 m by 10.5 m by 5.5 m in length, width and depth, respectively. The DT is typically used for resistance and propulsion tests.



Figure 1 Generic frigate (model no. 10296), length (L_{pp}) is 7891 mm.

There were four configurations that were studied in the present campaign:

- Case 1: Base case, with active propeller at nominal RPM (303 min^{-1}).
- Case 2: Propeller overload (RPM=347 min^{-1}).
- Case 3: Appended hull, with no propellers on the model.
- Case 4: Propeller overload, without rudders (RPM=347 min^{-1}).

The model was towed at 1.9 m/s in all cases.

Measurement device

The PIV measurement system used in the current study was built by MARIN to be used at full-scale and it is called 'FlowPike'. The device can be attached to the hull of a vessel to perform velocity measurements during sea trials (Figure 2). The FlowPike contains a 300 mJ double-pulse laser and two 5.5-megapixel cameras in a watertight housing. This combination of laser and cameras can capture (double-frame) images at 20 Hz. The measurement plane is ~1.4 m x 0.6 m and the center of the measurement plane is ~2.5 m away from the center of the FlowPike.

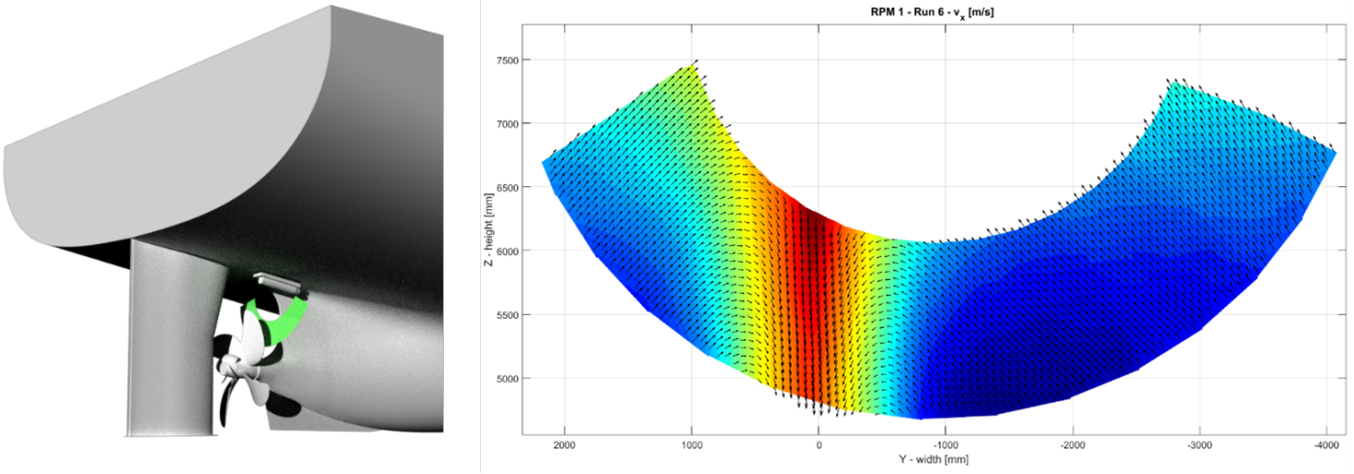


Figure 2 FlowPike full-scale measurement location (left) and results (right). The FlowPike can be rotated around its longitudinal axis to increase the total measurement area. This was done in the previous measurements, but in the present measurements the rotation angle was fixed.

The FlowPike has been operational since 2020. In 2020, acceptance tests have been conducted in the DT, see [9]. During these tests, the FlowPike was towed and the uniform flow was measured. In 2022, the FlowPike was used within the JoRes JIP (www.jores.net) to measure the inflow to a propeller at full-scale ([9], [10]).

As opposed to measurements at full-scale, the flow at model scale needed to be seeded. In the current measurements, polyamide particles (Orgasol ES6) with a mean diameter of approximately 60 μm were used. The seeding was injected into the water using a MARIN-designed seeding system.

Mounting and triggering

The FlowPike was mounted at a fixed location approximately halfway down the length of the basin to measure the flow during and after the passage of the model. This basin-fixed approach makes it possible to measure up to 12 ship lengths (L_{pp}) behind the vessel. The FlowPike was positioned such that it measures in a vertical plane oriented perpendicularly to the sailing direction. Being a stereo-PIV system, the FlowPike measures three components of velocity in each point of the measurement plane (2D-3C).

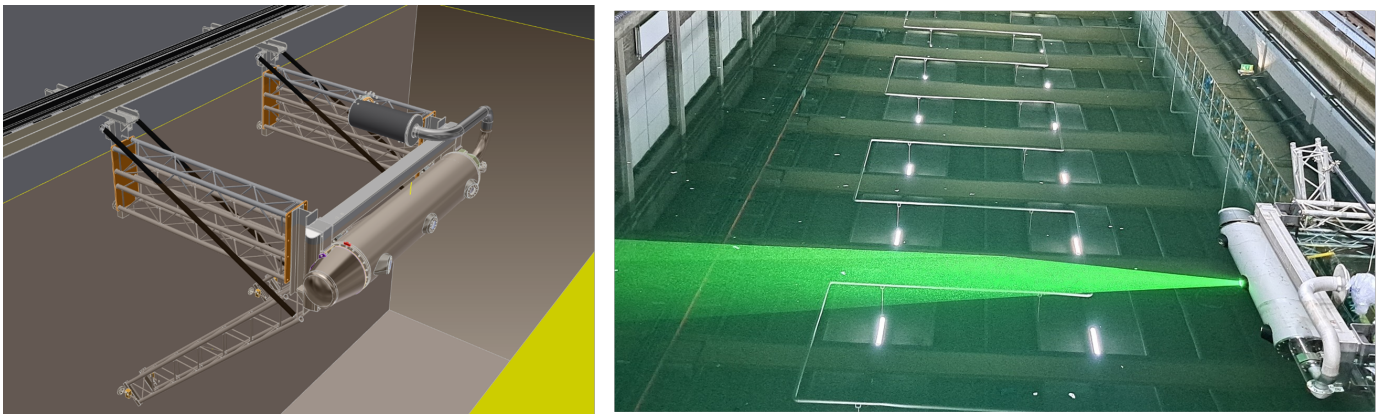


Figure 3 3D model of the mounting of the FlowPike to the basin wall (left). The waterline is indicated with a yellow line on the wall. FlowPike in the basin with laser sheet ON (right). It can be seen that the laser sheet reflects off the water surface approximately half way across the width of the basin.

The FlowPike was fixed to the wall of the basin using a frame to bring the FlowPike sufficiently close to the basin centerline. The FlowPike was submerged such that the line on which the cameras and the laser windows are is approximately 30 cm below the surface. The 10 m long cables of the FlowPike were long enough to have all the control boxes and the acquisition PC placed alongside the basin. The PC could be controlled from the basin carriage, which made it possible to run the PIV measurements remotely, i.e. from the carriage. The setup is presented in Figure 3.

The flexibility of varying the location of the measurement plane is a huge advantage of a basin-fixed system. Performing a measurement at e.g. $0.5 \cdot L_{pp}$ aft of the rudder stock is done in the same

way as a measurement at $4 \cdot L_{pp}$ and the only limitation that remains is the length of the basin. In the present campaign, the first measurement plane was recorded at $0.08 \cdot L_{pp}$ and the last at $12 \cdot L_{pp}$ for each run. Between these two, there was a measurement plane every 9.5 cm or 0.012 L_{pp} (corresponding to a 20 Hz measurement of a model moving at 1.9 m/s).

Importantly, each PIV measurement was started by a trigger fixed to the carriage; the trigger sends a signal to the PIV system when the carriage passes a certain position in the basin. Note, however, that this does not mean that each PIV shot is at the same relative position to the model in every run (i.e. the model and the PIV system are not synchronized). This is because the PIV system is running at 20 Hz using its internal clock, with the measurement sequence starting on the first PIV shot that comes after the trigger signal. In practice, this means that there is a variability between the position of the PIV measurement planes with respect to the model position that is smaller than the distance travelled by the model in 1/20 s (1/f s); this distance is <9.5 cm. This variability was quantified for each run by estimating the relative position of the laser sheet and a recognizable feature on the model in a certain frame in the measurement sequence (frame 39). In this frame, the laser sheet was seen hitting the rudder at slightly different places for each run. Knowing that the total variability is 9.5 cm, the offset for each run was estimated by eye, rounded off to the nearest centimeter. These data are then assigned as an offset to all frames in each run, relating them in that way to a zero *x*-position that was chosen to be the rudder stock.

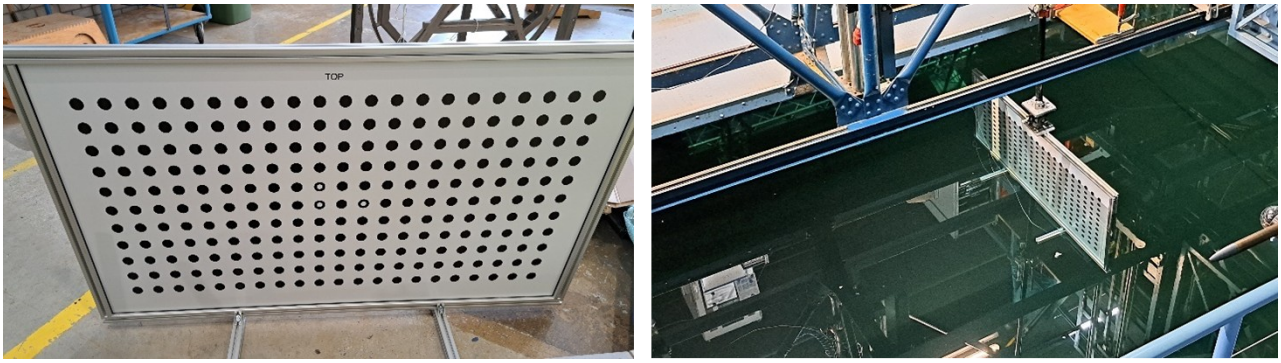


Figure 4 Calibration plate (left); calibration plate positioned in the measurement plane in the basin (right).

Calibration

The calibration was performed using a calibration grid of 1.75 m by 1.0 m (Figure 4). The board is white, with black painted dots of 37.5 mm diameter, spaced 75 mm apart. The board is flat and it has dots painted on both sides; the thickness is 4 mm. The calibration was performed in the position of the laser sheet, in the middle of the DT. Images were recorded in this position, as well as with the board slightly rotated; this is a requirement of the calibration procedure.

The calibration and subsequent recording and processing of images was done using LaVision's Davis 10.2.1 software. In addition to the basic calibration of the camera system, stereo self-

calibration was performed. The procedure resulted in improved calibration, indicating that there was an initial misalignment. Overall, the resulting calibration is considered satisfactory and on a similar level to previous measurements with the FlowPike.

PIV recordings

A normal run consisted of 1100 image pairs captured at 20 Hz; the number of runs was between 26 and 40 depending on the case. Although it is a challenge to achieve good seeding quality in a towing basin, this was managed by seeding the flow on every return run. This made it possible to finally process the data with 32x32 px^2 interrogation windows, with 50% overlap.

The flow under study contained relatively large velocity gradients. Another unfavorable effect is the fact that the dominant flow direction (created by the propeller outflow) is oriented through the light sheet plane. Both effects lead to loss-of-correlation in PIV processing. Besides this, images captured right behind the model (say at $0.1 \cdot L_{pp}$) will have a large velocity and require a short inter-frame time (Δt), while those captured far away from the model (e.g. at $10 \cdot L_{pp}$) will have a much lower velocity and therefore require a larger Δt. In theory, the Δt would need to be optimized to provide on average the same pixel displacement in all images. This was not achieved, since it was not possible to program a different Δt for each PIV recording. Instead, in the current measurements, we made multiple runs at the same flow conditions using Δt values ranging from 250 μs to 20000 μs. This was done in an attempt to combat all the unfavorable effects listed above, and specifically to have a high accuracy of velocity in all areas of the flow and at all $-x/L_{pp}$ values. Naturally, in some runs with e.g. a large Δt, there were areas of the flow right behind the propeller where it was not possible to obtain valid velocity vectors and which therefore remained empty. Likewise, it is expected that in runs with a small Δt the velocities obtained far away from the propeller were less accurate. Despite this, the varying Δt values combined with the advanced multi-level processing algorithms that reduce the interrogation window size during processing made it possible to minimize the inaccuracies and adequately resolve the flow at all measurement positions.

Data processing

As mentioned, the data was processed using a multi-level processing algorithm that starts with interrogation area size of 64x64 px^2 (1 pass, 50% overlap, square interrogation windows) and reduces to 32x32 px^2 (2 passes, 50% overlap, adaptive interrogation windows) for the final passes. In between, standard outlier detection procedures are applied. In a post-processing step, outliers are eliminated again, and places where a single or a limited number of vectors were missing were filled in by interpolation using the data from the surrounding vectors. In this way, the final PIV

images contained empty areas only where the velocity was too high for a given Δt, which was normally at the position of the propellers. No data smoothing was applied in the end. The resulting resolution of the measurements is one vector every 4.74 mm (1.5% of the propeller diameter). The size of the vector grid is 365x178; in physical dimensions, this amounts to 1730x844 mm^2. This corresponds to 152% of the model width and to 273% of the draught.

The raw vector fields were exported from Davis and further processed using in-house Python scripts. The processing consisted of assigning the correct XYZ position to each vector and to averaging the data. The XYZ position was referenced to a zero-position placed at the rudder stock (x), the centerline (y) and the water surface (z); x is positive in the sailing direction, y is positive towards the port (left) side and z is positive vertically upwards. The zero-position is therefore fixed to the model, however, the velocity vectors were kept in the basin-fixed coordinate system, which means that the velocities are generally close to zero (reflecting the stagnant water of the basin).

For each configuration (Cases 1-4), the average velocities in all three directions, the average velocity fluctuations and the turbulence kinetic energy were calculated at 18 x/L_{pp} positions. These positions were: -0.08, -0.1, -0.15, -0.2, -0.3, -0.4, -0.5, -0.6, -0.8, -1, -1.5, -2, -3, -4, -6, -8, -10 and -12. Finally, the mean vorticity in the x-direction was calculated using the mean velocity fields in the YZ-plane calculated previously.

PIV measurement uncertainty

PIV measurement uncertainty is notoriously difficult to quantify since the measurement chain consists of several digitization, transformation, filtering and correlation steps. It is common to quantify the uncertainty in detailed laboratory studies, while in studies such as the present one only an indication of uncertainty is given.

In previous measurements using the FlowPike, the uncertainty was derived by comparing the PIV measurements with the known uniform flow. This difference indicated that there is a systematic component to uncertainty linked to the peak-locking effect and possible calibration plate misalignment. The uncertainty amounted to 2.4%, 1.7% and 7.8% for the axial, lateral and vertical components of the mean velocity, respectively [10]. Additionally, there was a small random component that came from the finite number of images used in calculating the average velocity; this was smaller than 0.3% for all the velocity components.

In the present measurements, it is expected that there are three sources of error:

1) Peak-locking error, which is expected to be most pronounced in parts of the flow where the water is quiescent. In the current measurements, this is away from the hull-propeller region (below and to the sides) before the velocity disturbances introduced by the model spread to those regions (i.e. at low $-x/L_{pp}$ values). The peak-locking error is related to the observed

particle shift which also depends on the selected Δt. It is expected that this error is reduced since multiple Δt values were used for each case and the results were averaged. However, the order of magnitude of the uncertainty is expected to be the same as the numbers cited above.

2) It is expected that there is a residual effect of the misalignment of the calibration plate with respect to the laser sheet that was not corrected by the self-calibration procedure. This effect is likely non-uniform across the field of view.
3) Finally, an important source of uncertainty comes from the limited number of runs that were done in each case. Since only measurement planes recorded at approximately the same x/L_{pp} can be averaged together and the number of runs was 26-40, this means that a relatively small number of measurements was used to calculate the mean. Generally, several hundred measurements are necessary for an accurate mean velocity and several thousand are necessary for accurate turbulence statistics. In the present measurements, the uncertainty of the mean is: ±16% for the *u*-component, ±73% for the *v*-component and ±27% for the *w*-component. It is expected that this is the dominant source of error.

Despite this, the results that were obtained in the current study appear consistent, making it possible to use the mean velocity value for comparison with CFD. Fluctuating components should be used with caution.

3. Results

The complete dataset consists of velocity fields measured in each run in all the four cases. The fields contain raw 3D velocity vectors along with their physical position in space. Since the dataset is large, the data are processed further to obtain a smaller set that contains average quantities at selected x/L_{pp} positions. These data are smaller and more easily handled in CFD comparisons.
Examples of results are presented next. Figure 5 shows the longitudinal velocities in the measurement plane of Case 1. Here, the axes were scaled by the model width (1048.4 mm) and the draught (309.1 mm) while the velocity was scaled with the towing speed (1.9 m/s). The wake field generated by the twin propellers is clearly visible in the first few plots, while at locations further away from the model the wake field gradually loses form and subsides. Near the free surface and the centerline the positive velocities correspond to the wake of the hull. Due to the rotation of the propeller slipstream, this hull wake is convected to large depth further downstream.

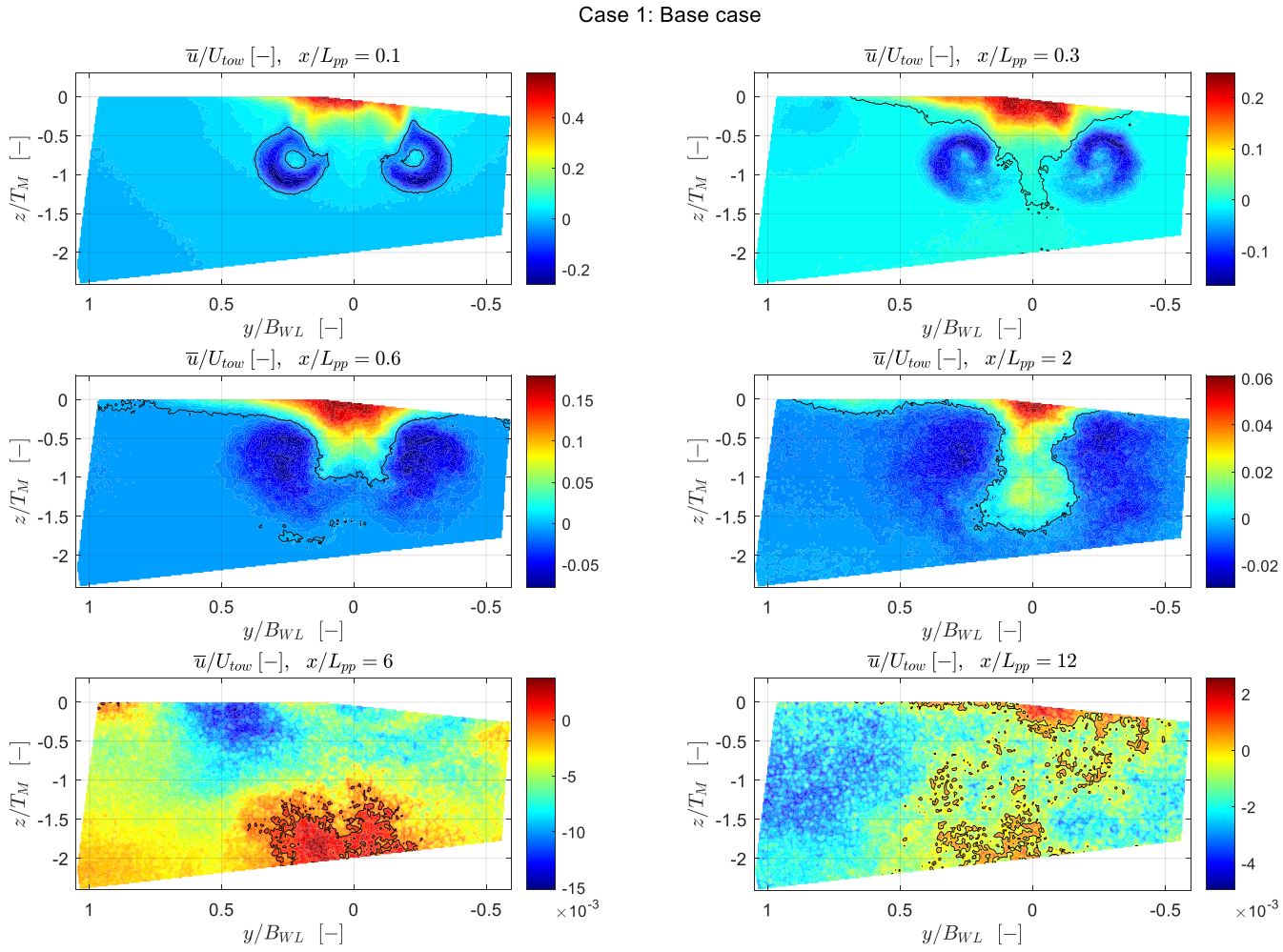


Figure 5 Mean longitudinal velocity in the Base case (Case 1) at various -x/L_{pp} locations. The zero velocity positions are indicated with a solid black line. Note the changing velocity scale.

For comparison, Case 3 (Appended hull) is shown in Figure 6. Since in this case the model does not have propellers, a different flow field is measured. The main disturbance to the quiescent water in the basin is now caused by the hull displacement and its boundary layer inducing flow in the positive longitudinal direction only. Contrary to Case 1, the flow remains symmetrical at large downstream distances from the stern.

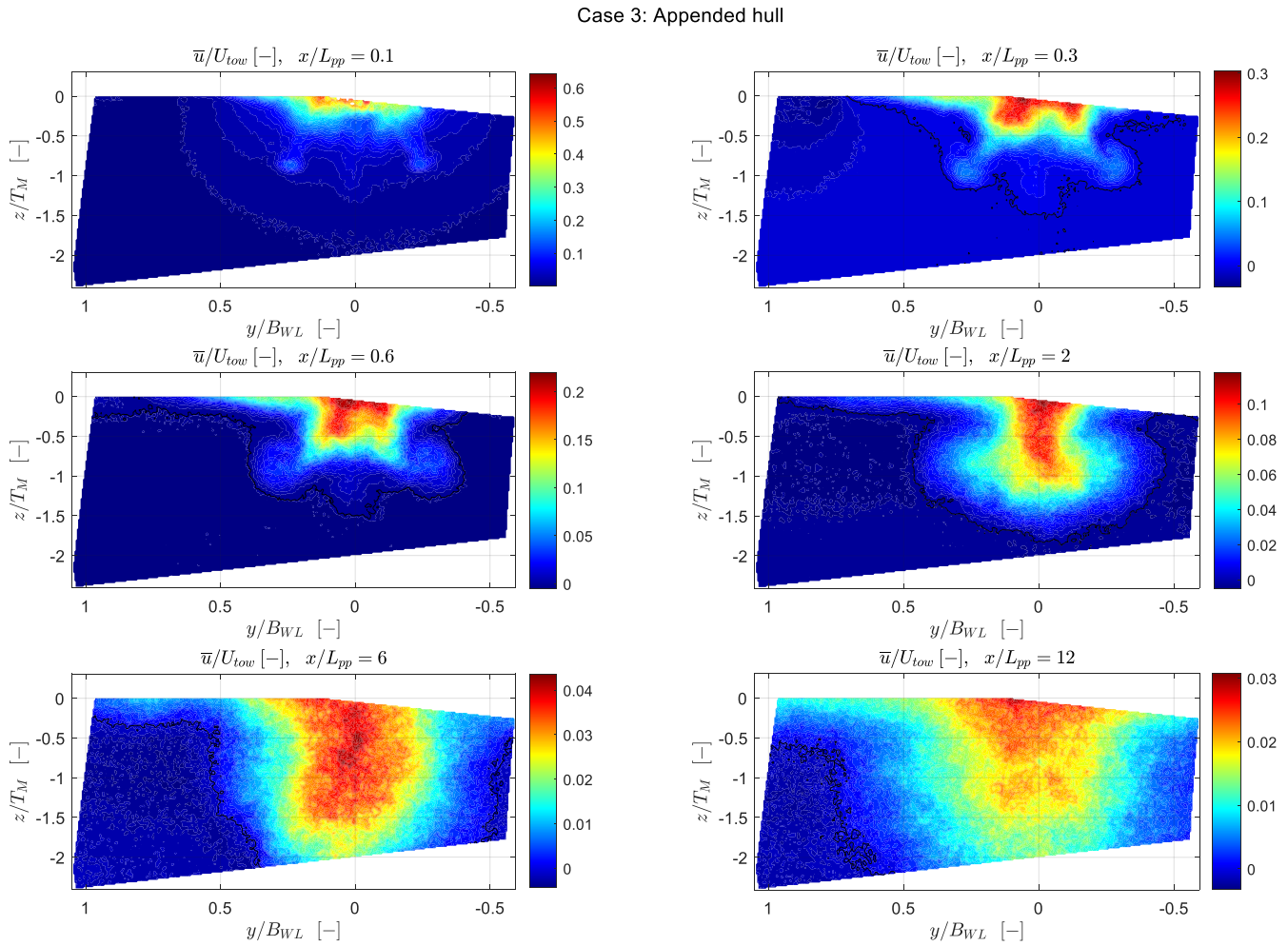


Figure 6 Mean longitudinal velocity in the Appended hull case (Case 3) at various -x/L_{pp} locations. The zero velocity contour is indicated with a solid black line. Note the changing velocity scale.

A comparison of longitudinal velocity between the four measured cases is made in Figure 7 for -x/L_{pp}=0.3 and in Figure 8 for -x/L_{pp}=2. The velocity scale is the same, making it possible to observe the differences between the cases.

The most obvious difference is between the powered cases (1, 2 and 4) versus the unpowered case 3; cases 1, 2 and 4 have a component of velocity directed towards the aft, while case 3 only induces forward directed flow. Another difference comes from the presence or the absence of rudders; cases 1, 2 and 3 have rudders, while case 4 does not. The rudder induces a characteristic flow pattern, which is especially visible when comparing case 2 with case 4; case 4 with no rudders has a circular pattern of the propeller vortex, while case 2 has a more irregular shape of the propeller-induced flow.

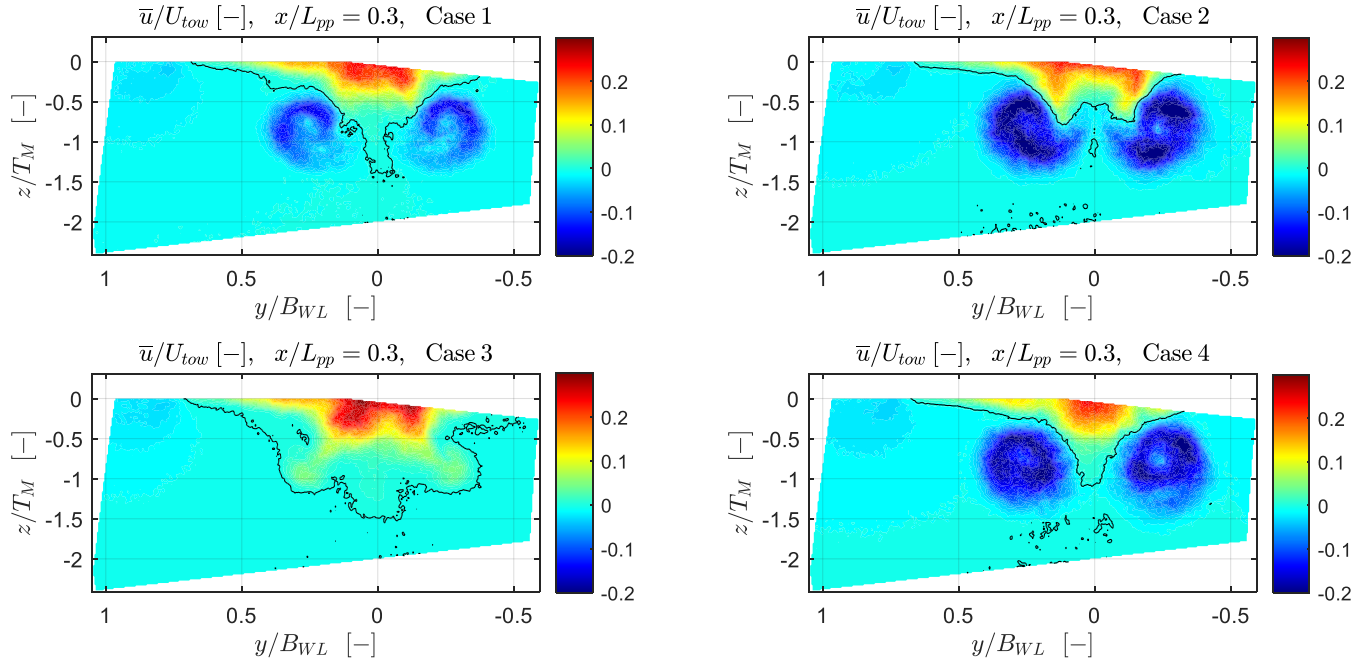


Figure 7 Longitudinal velocity comparison between cases 1-4 at -x/L_{pp}=0.3.

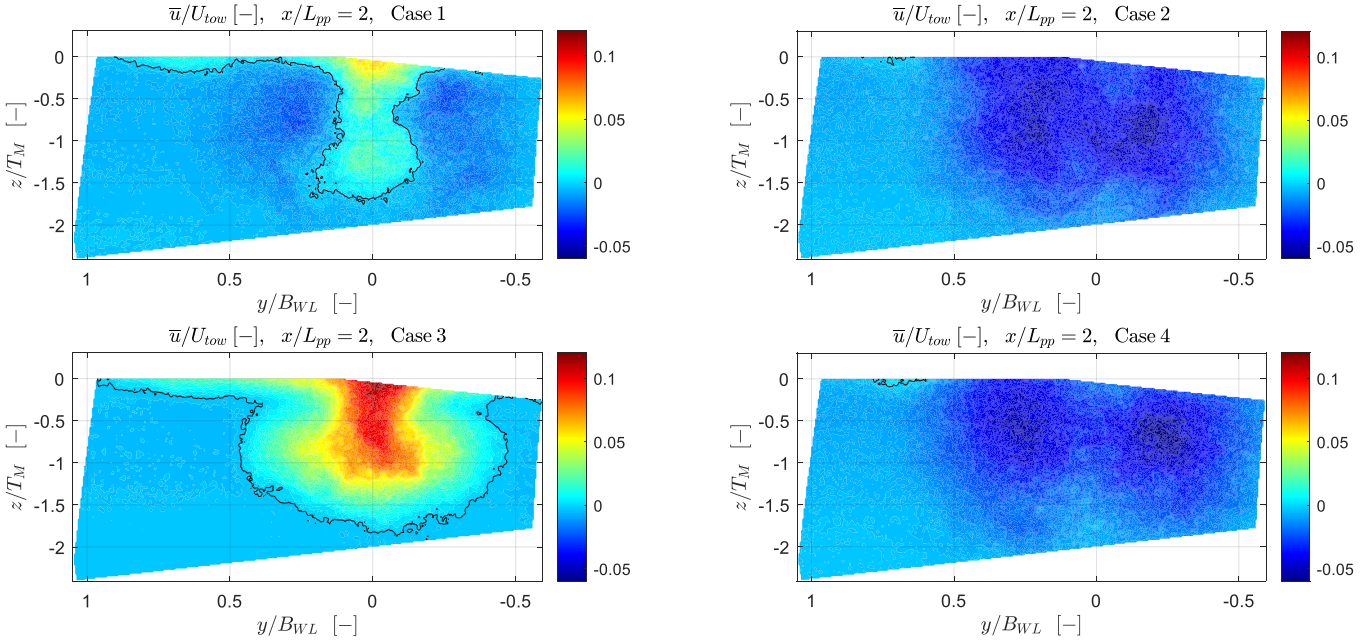


Figure 8 Longitudinal velocity comparison between cases 1-4 at -x/L_{pp}=2.

The longitudinal velocity fluctuations for case 1 are shown in Figure 9. Note that the computed velocity fluctuations and the computed turbulent kinetic energy are resulting both from turbulence as well as from the circumferential mean velocity variations in the slipstream of the five-bladed propeller. As expected, the fluctuations are largest directly behind the propellers, reducing and losing the propeller outline at -x/L_{pp}>1. Similar plots are made with turbulent kinetic energy as well as with quantities derived from the mean velocity such as vorticity (not shown).

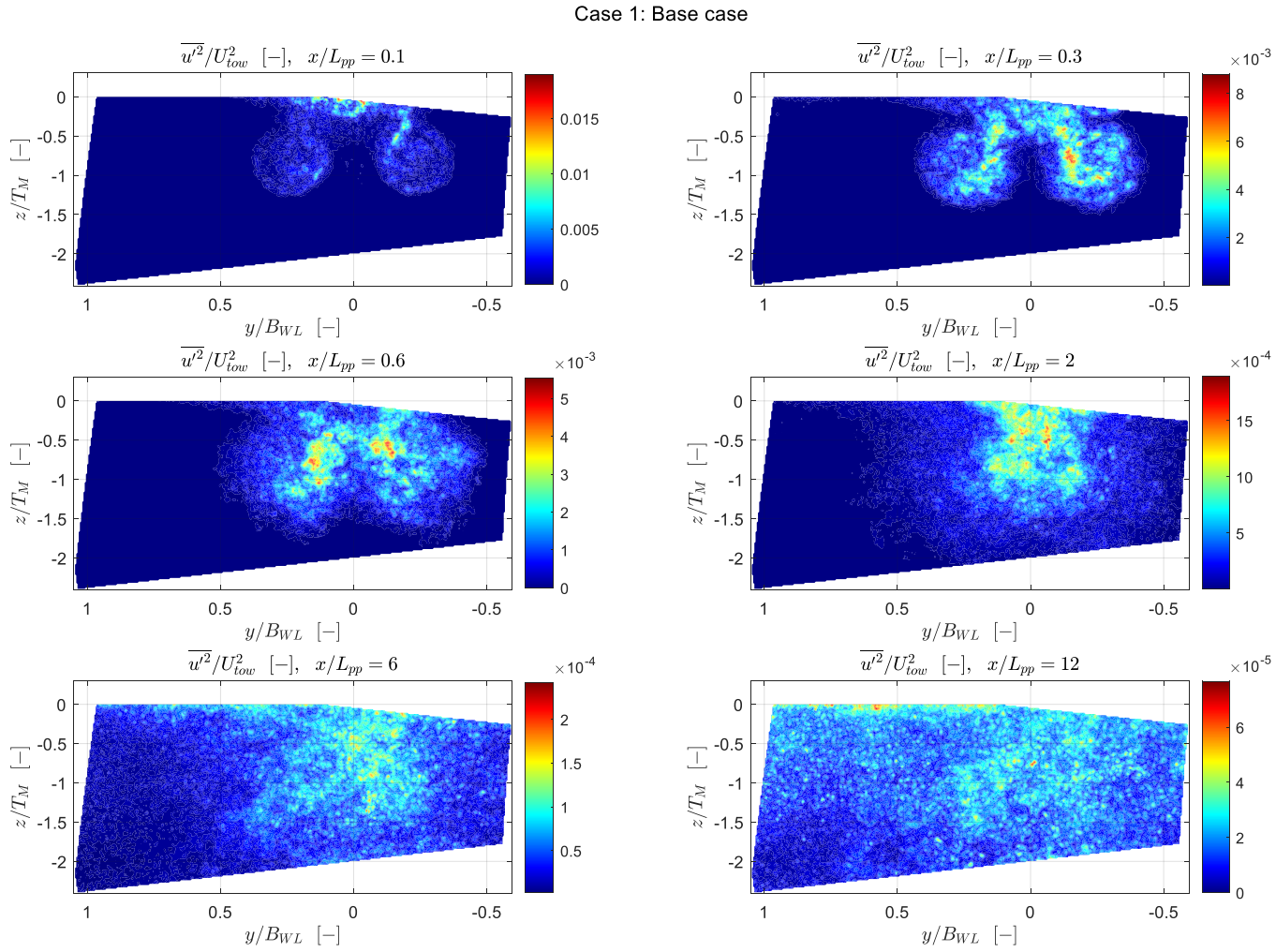


Figure 9 Longitudinal velocity fluctuations in the Base case (Case 1) at various -x/L_{pp} locations. Note the changing velocity scale.

Another way of presenting the current data is to derive mean or maximum quantities in a certain part of the measurement area. This is shown in Figure 10. The mean and maximum values obtained in this way are plotted against the -x/L_{pp} position of the measurement.

Example of this kind of data is shown in Figure 11 and Figure 12. Figure 11 presents the turbulent kinetic energy at 18 distances behind the model for all cases; the TKE is scaled with the square of the towing speed. Both the maximum and the mean plots show the same relative intensities of the TKE between the cases. Namely, the lowest values of TKE close to the model are measured in the Appended hull case, followed by the Base case and the two cases with high RPM (Propeller overload and No rudders case). At larger distances behind the model, the Base case has the lowest TKE value, followed by the Appended hull case and the two higher RPM cases.

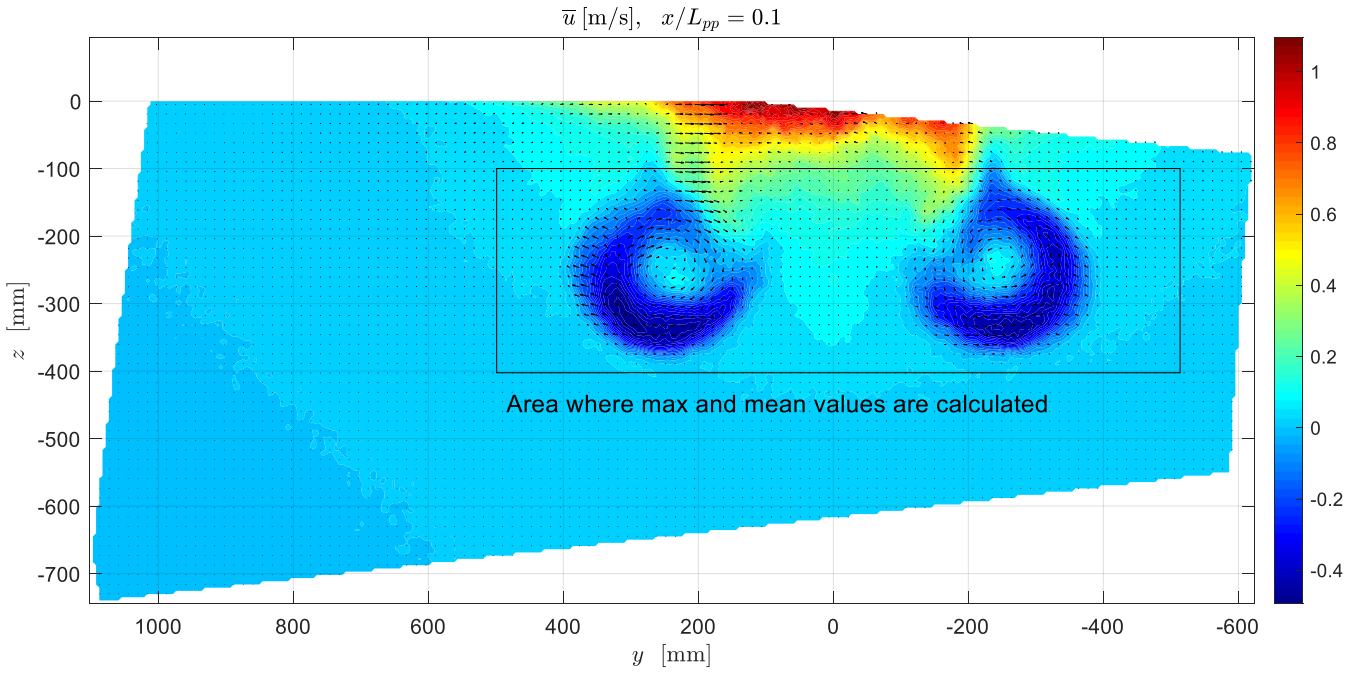


Figure 10 Part of the measurement area in which the mean and maximum velocity are calculated (black rectangle).

Initially, it was thought that this was caused by the different cases having runs with slightly different Δt; e.g. some cases had a few more short-Δt runs and others had more long-Δt runs. The mean data was then re-calculated for all cases by using a selection of runs that had the same Δt in all cases. This showed that Δt had no influence on the observed effect. Since no other sources of bias could be identified, it could only be concluded that the observed effect is physical. In fact, the most interesting observation is not that the Base case has a lower value of fluctuations at high -x/L_{pp} (far away from the model), but that the Appended hull case has a high value at those locations. Furthermore, the Appended hull case has a peak fluctuation value downstream of all the other cases. When looking at data like this, the powered cases (Base, Propeller overload and No rudder cases) are consistent with each other, while the Appended hull case differs. The reason for this difference is unknown although it is to be expected, since the Appended hull case uniquely does not have a propeller and therefore introduces flow only in the sailing direction.

The breakdown of TKE into individual contributions of the velocity components is shown in Figure 12. In general, u and w components are of similar magnitude, while the v component is larger, probably caused by the much larger uncertainty in the measurement of the v-component, as discussed previously.

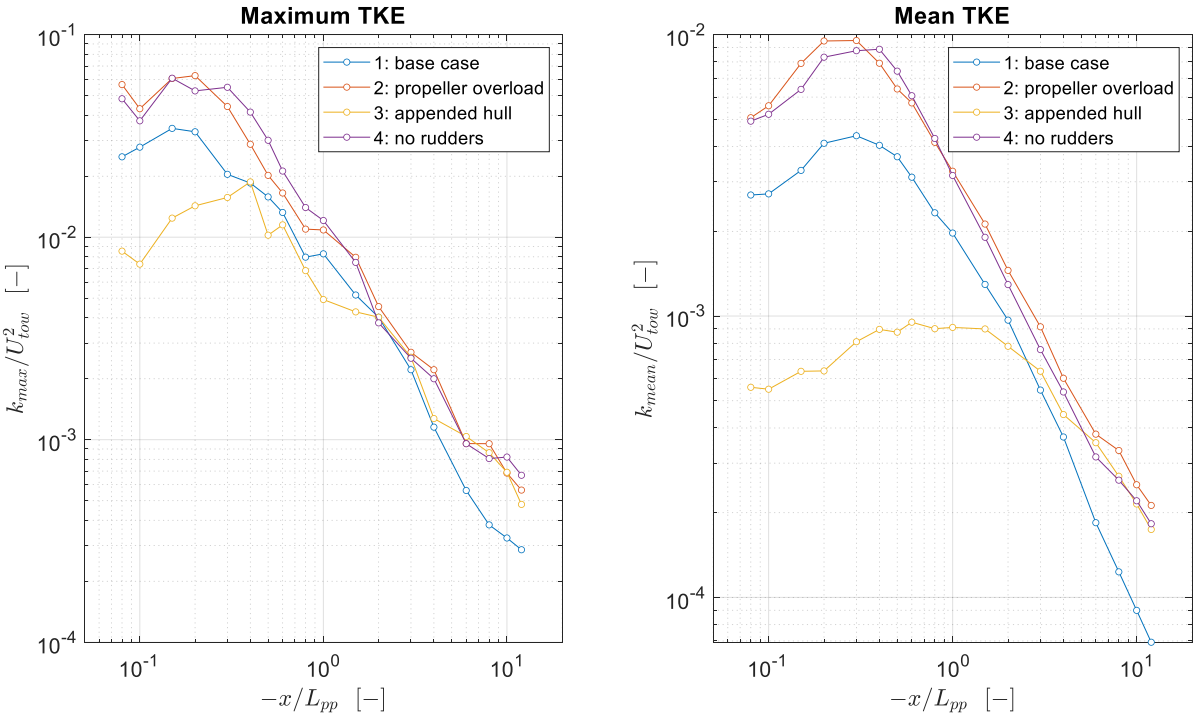


Figure 11 Maximum and mean turbulent kinetic energy at various distances behind the model for all the four cases. The area where max and mean are calculated was defined previously (see above).

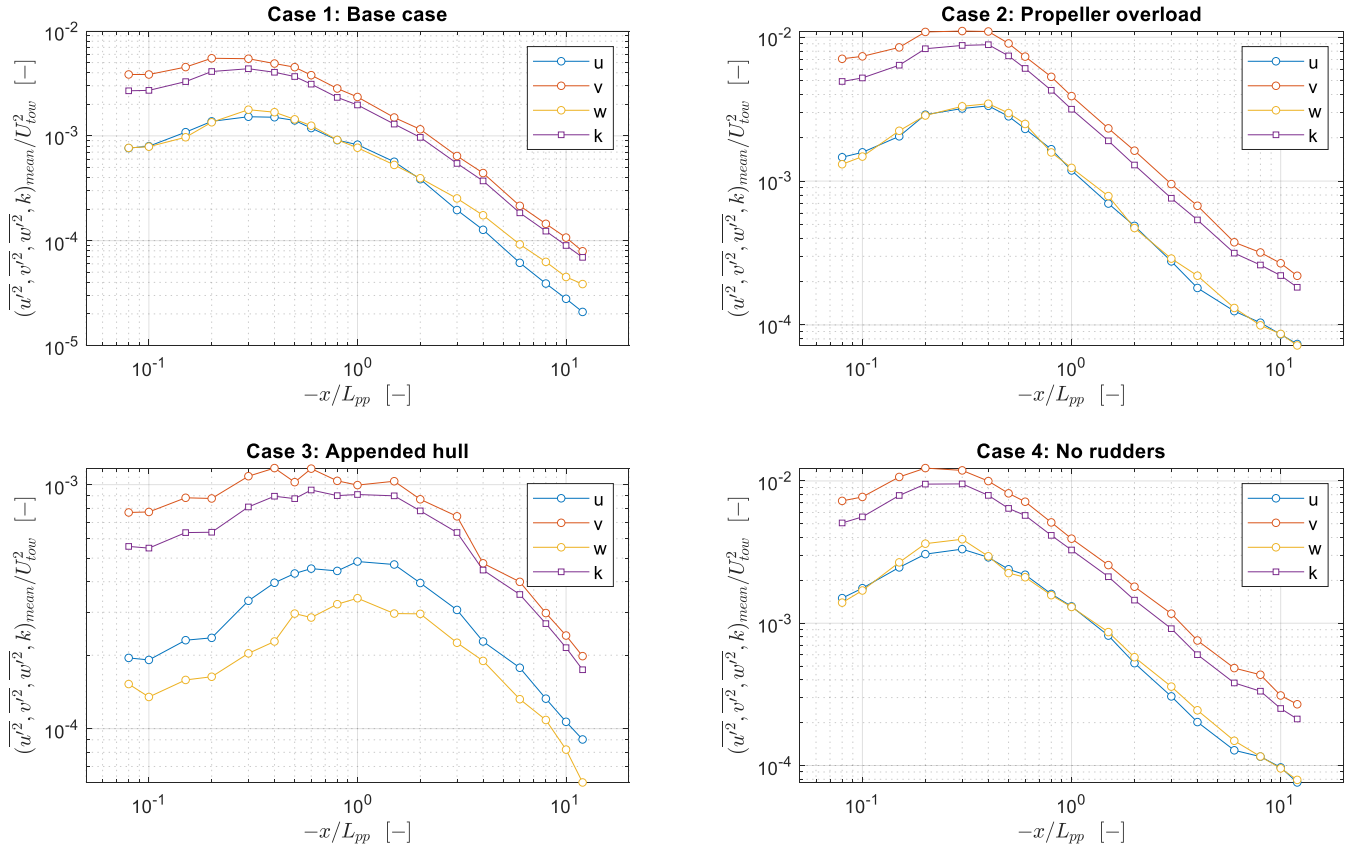


Figure 12 Mean velocity fluctuations at various distances behind the model for all the four cases. The area where the mean is calculated was defined previously (see above).

4. Conclusions

The following conclusions can be drawn from the current study:

- Successful measurements of the wake field behind a twin-screw frigate model have been performed in MARIN's Deepwater Tank. Three components of velocity were measured in a large transverse plane that covers the entire wake field. Measurements were performed from very close to the model until twelve ship lengths away. For these measurements the FlowPike full-scale PIV measurement system was used for the second time in the basin. The device performed well, i.e. in the same way as intended when first developed. The performed measurements deliver good insight into the flow behind the vessel. The resulting data can be used to validate CFD.
- The quality of the resulting mean velocities is satisfactory in general, however, there is a difference in uncertainty for different components of velocity. Longitudinal and vertical velocity components have an acceptable uncertainty, while the lateral component is poor. This is likely a result of the combination of systematic sources of error (pixel locking and calibration plate misalignment) and a random error coming from the limited number of measurement runs in each case. The low number of runs is a serious limitation of the current measurement configuration (basin-fixed PIV system), but a sufficiently large number of runs would require prohibitively long basin time.

Recommendations

- It is recommended to take sufficient time to carefully calibrate the FlowPike to minimize the need to correct the calibration later using the self-calibration procedure, or to make the correction easier and more accurate.
- The overlapping of the measurement planes can be improved if the PIV system operates in 'cyclic mode'. This is done by triggering the first cycle with the carriage and then making the first cycle continue until the model is at the end of the basin.
- It is recommended to use the derived second-order statistics with caution, since their accuracy is relatively low.

Acknowledgments

The support of the Dutch Ministry of Defense of this work is gratefully acknowledged.

References

[1] L. Gui, J. Longo and F. Stern, "Towing tank PIV measurement system and data and uncertainty assessment for DTMB Model 5512," in *Proc. The Third International Workshop on PIV'99*, Santa Barbara, USA, 1999.

[2] J. Tukker, J. J. Blok, G. Kuiper and R. H. M. Huijsmans, "Wake flow measurements in towing tanks with PIV," in *9th Int. Symp. on Flow Visualization* , Edinburgh, UK, 2000.

[3] B. G. Paik and S. J. Lee, "PIV Analysis of Wake behind a Container Ship Model with a Rotating Propeller," in *5th Int. Symp. on Particle Image Velocimetry*, Busan, Korea, 2003.

[4] J. Y. Lee, B. G. Paik and S. J. Lee, "PIV measurements of hull wake behind a container ship model with varying loading condition," *Ocean Engineering,* vol. 36, pp. 377-385, 2009.

[5] J. H. Seo, D. M. Seol, T. G. Lim, S. T. Park, B. W. Han and S. H. Rhee, "A stereo PIV measurement of a model ship wake in a towing tank with uncertainty assesment," in *10th Int. Symp. on Particle Image Velocimetry*, Delft, The Netherlands, 2013.

[6] J. H. Seo, D. M. Seol, B. W. Han and S. H. Rhee, "Turbulent wake field reconstruction of VLCC models using two-dimensional towed underwater PIV measurements," *Ocean Engineering,* vol. 118, pp. 28-40, 2016.

[7] T. Wu, L. W, D. Jiang, R. Deng and Y. Li, "Stereo Particle Image Velocimetry Measurements of the Wake Fields Behind A Panamax Bulker Ship Model Under the Ballast Condition," *J. Mar. Sci. Eng.,* vol. 8, no. 6, p. 397, 2020.

[8] J. Longo, J. Shao, M. Irvine and F. Stern, "Phase-Averaged PIV for the Nominal Wake of a Surface Ship in Regular Head Waves," *J. Fluids Eng.,* vol. 129, no. 5, pp. 524-540, 2007.

[9] M. Birvalski, G. D. Struijk and D. Ponkratov, "Full-Scale PIV Measurements of the Propeller Inflow," in *15th Int. Symp. on Particle Image Velocimetry*, San Diego, US, 2023.

[10] M. Birvalski, S. L. Toxopeus, G. D. Struijk and D. Ponkratov, "Comparison of full-scale PIV measurements with CFD simulations of a ship propeller inflow," in *21st Int. Symp. on Appl. of Laser and Imaging Techn. to Fluid Mech.*, Lisbon, Portugal, 2024.